## Discussion of Flap-Lag Dynamics of Hingeless Rotor Blades

Today's discussion is on how one can make practical use of the model (and slightly extended versions thereof) we developed in class during the past three lectures. The figures in this handout are lifted from [1], [2], and [3]. A simplified version of our model is developed in [1], and many results both for elastically coupled and uncoupled blades are presented. The main conclusion is that elastic coupling, as defined by the parameter $R$, has a strong influence. Experimental verification of the model came with a surprise. Nonlinear aerodynamics had a much more significant effect than anyone had thought: Because of the model scale, the Reynolds number was low enough that static stall actually induced an instability [2]. This is not something we worry about in full-scale aircraft. Finally, the model was extended in [3] to allow much larger elastic coupling by tilting the spring-restrained hinges at angles up to 45° while leaving the blade at flat-pitch orientation. This large elastic coupling, in conjunction with negative pitch-lag coupling (pitch decreases as blade leads), allowed the lead-lag damping to be made orders of magnitude larger than before. Unfortunately, no combination of parameters was found that would eliminate the instability for the blade *and, simultaneously*, eliminate ground/air resonance instabilities for a coupled rotor-fuselage system. Additional work has been done on this by various researchers, including Prof. Gandhi at Penn. State.

## References


[1] Ormiston, Robert A. and Hodges, Dewey H., "Linear Flap-Lag Dynamics of Hingeless Helicopter Rotor Blades in Hover," *Journal of the American Helicopter Society*, Vol. 17, No. 2, April 1972, pp. 2 – 14.

[2] Ormiston, R. A. and Bousman, W. G., "A Study of Stall-Induced Flap-Lag Instability of Hingless Rotors," *Journal of the American Helicopter Society*, January 1975.

[3] Ormiston, Robert A., "Concepts for Improving Hingeless Rotor Stability," In *Proceedings of the American Helicopter Society Mideast Region Symposium*, Essington, PA, August 1976.

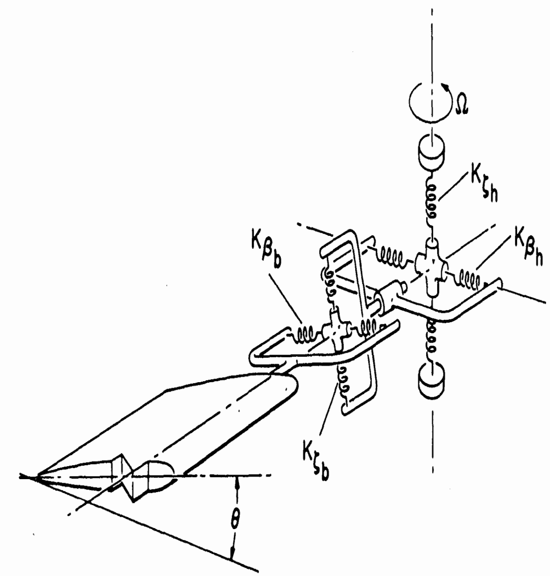


FIGURE 14. Arrangement of flap and lead-lag springs of rotor blade and hub for simulating variable elastic coupling. For clarity, rotor blade springs shown radially displaced from axis of rotation.

untwisted blades

$$M_{\beta_{aero}} = \frac{\gamma I \Omega^2}{8}\left\{\theta - \left(1 + \frac{c_{d_0}}{a}\right)A + \left[2\theta - \left(1 + \frac{c_{d_0}}{a}\right)A\right]\frac{\dot{\zeta}}{\Omega} - \left(1 + \frac{c_{d_0}}{a}\right)\frac{\dot{\beta}}{\Omega}\right\} \quad (39)$$

$$M_{\zeta_{aero}} = -\frac{\gamma I \Omega^2}{8}\left\{\frac{c_{d_0}}{a} + A\theta - C + \right.$$

$$\frac{\dot{\zeta}}{\Omega}\left(2\frac{c_{d_0}}{a} + A\theta\right) + \frac{\dot{\beta}}{\Omega}(\theta - 2A)\Big\} \quad (40)$$

flexibility. Previous studies have treated (
coupled configuration, where all flexibility
in the hub spring system.

The configuration of Fig. 14 reduces
equivalent single spring system at zero
which defines the rotor blade nonrotating
The equivalent spring system is given by

$$K_\beta = \frac{K_{\beta_B} K_{\beta_H}}{K_{\beta_B} + K_{\beta_H}}, \quad K_\zeta = \frac{K_{\zeta_B} K}{K_{\zeta_B} +}$$

The complete elastic moments can be writ

$$M_{\beta_{elastic}} = -\frac{\beta}{\Delta}\left[K_\beta + R(K_\zeta - K_\beta \sin^2\theta\right] \cdot$$

$$\frac{\zeta R}{2\Delta}(K_\zeta - K_\beta)$$

$$M_{\zeta_{elastic}} = -\frac{\zeta}{\Delta}\left[K_\zeta - R(K_\zeta - K_\beta)\sin^2\theta\right] -$$

$$\frac{\beta R}{2\Delta}(K_\zeta - K_\beta)$$

where

$$\Delta = 1 + R(1 - R)\frac{(K_\zeta + K_\beta)}{K_\zeta K_\beta} \text{ si}$$

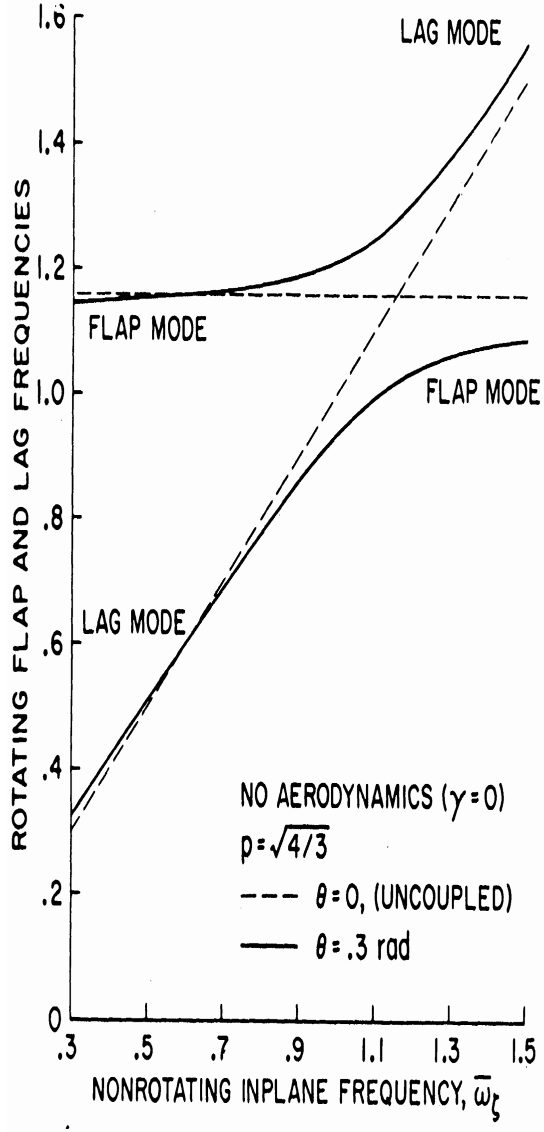


FIGURE 10. Effect of elastic coupling on rigid hinged blade flap and lead-lag frequencies without aerodynamics, R = 1.0.

Figure 12 further illustrates this effect as a function of collective pitch for a specific configuration.

6) The flapping response phase for $1P$ pitch excita tion is significantly altered by elastic coupling. Thi implies that coupled rotor-fuselage dynamic equation should include the rotor blade inplane degree of free dom.

7) The rigid hinged blade gives a reasonably accu rate approximation of the actual elastic blade stabilit if the elastic coupling effects are properly accountec for.

## APPENDIX

A brief derivation of the aerodynamic forces and equations of motion for both the rigid hinged blade and the elastic blade are given below. The basic $x$, $y$, $z$ rotating coordinate system in Fig. 13 shows the positive conventions for angular $(\beta,\zeta)$ and linear $(u,v,w)$ displacements (except a negative $u$ displacement is shown).

### AERODYNAMIC FORCES

The $y$ and $z$ components of the aerodynamic loading (lb/ft) can be written as follows

$$dF_z = dL - \phi dD \qquad dF_y = -dD - \phi dL \quad (30)$$

The elemental lift and drag forces can be written from simple strip theory. Since $\alpha = \theta - \phi$ and $\phi \simeq U_P/U_T$ for small inflow angles

$$dL = \frac{\rho ac}{2} V^2 \left(\theta - \frac{U_P}{U_T}\right) dx \qquad dD = \frac{\rho c V^2}{2} c_{d_0} dx \quad (31)$$

$= p^2, \; W = \bar{\omega}_\zeta^2, \quad \eta = \gamma/8 \qquad (11)$

immediately follow since $c_{d_0} > 0$, essary (but not sufficient) condition at $1 < p^2 < 2$. This indicates that otors without hinge offset or $\delta_3(p =$ ble. This does not mean that de- coupling is not present, but only be sufficient to cause instability. flap frequency ($p$) the minimum ral stability, $\theta_{min}$, occurs when $\bar{\omega}_\zeta =$ t of Lock number.

$= [P^2D/2(P - 1)(2 - P)] \qquad (12)$

minimum can be obtained for $p =$ will be referred to as $\theta^*$ and is de- profile drag coefficient and induced . For $a = 2\pi$

$2\sqrt{c_{d_0}/\pi}, \quad p = \bar{\omega}_\zeta = \sqrt{4/3} \qquad (13)$

specifies the lowest possible pitch hingeless rotor blade can become -lag oscillations.

ng is easily incorporated by modify- ping coefficient $C_{\dot{\zeta}}$.

$\left[\frac{2c_{d_0}}{a} + 2\eta_m \frac{\bar{\omega}_\zeta}{\gamma/8} + A\theta\right] \qquad (14)$

respectively the profile drag damp- ping, and induced drag damping. eters $1/2\%$ structural damping ($\eta_m$ order of 3 times the profile drag ld significantly increase $\theta^*$.

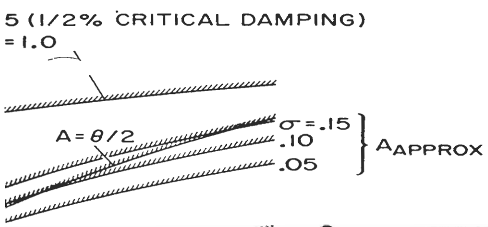


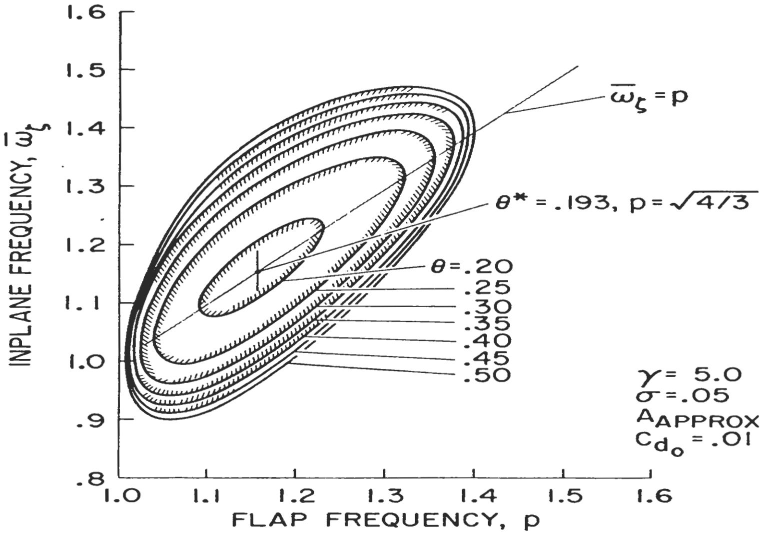


FIGURE 4. Stability boundaries for basic rigid blade equations.

Figure 3 illustrates the relationship between inplane damping and $\theta^*$ given by Eq. (13) including the effects of structural damping and various approximations for the induced inflow parameter $A$.

A summary plot giving basic flap-lag stability boundaries as a function of the flap and lead-lag frequencies is given in Fig. 4. For a particular collective pitch, the region of instability lies within the respective contour. These results illustrate the occurrence of $\theta_{min}$ for a given value of $p$ when $\bar{\omega}_\zeta = p$ and $\theta^*$ when $p = \sqrt{4/3}$.

*Case II, Effect of Pre-cone, No Elastic Coupling*

With pre-cone, the perturbation equations are identical to those used previously although the coning now becomes

$$\beta_0 = [\gamma/8](\theta - A)/p^2 + (p^2 - 1)\beta_{pc}/p^2 \qquad (15)$$

Routh's criteria yields the following expression for the collective pitch for neutral stability.

$$(\theta - A)^2 = \frac{P^2}{2(P - 1)(2 - P)} \times$$

*astic Coupling*

nogeneous equations for this case,
ndix are

$$-sF_{\dot{\zeta}} + F_{\zeta} \Big] \Big\{ \begin{matrix} \Delta\beta \\ \Delta\zeta \end{matrix} \Big\} = 0 \quad (22)$$
$$s^2 + C_{\dot{\zeta}}s + C_{\zeta} \Big]$$

ıg terms $F_{\zeta}$ and $C_{\beta}$ produce cross -lag moments proportional to lead- ons respectively. Previous studies .ected these terms in simplified analyses. However, as will be seen pronounced effects on the stability cteristics of rotor blade flap-lag tch angles $F_{\zeta}$ and $C_{\beta}$ are given by

$$R(\bar{\omega}_{\zeta}^2 - \bar{\omega}_{\beta}^2)\theta \qquad (23)$$

›roportional to pitch angle and is lent by virtue of the nonrotating equencies $\bar{\omega}_{\zeta}$, $\bar{\omega}_{\beta}$, and the variable ımе $R$.

ng of actual hingeless rotor blades particular design configuration and ribution of flexibility radially in- of the pitch bearing. As explained s characteristic is introduced in the s by dividing the flap and lead-lag ;wo separate spring systems, one er outboard of the pitch axis. The pling is denoted by $R$ and is pro- ction of flexibility present in the ard of the hinge axis.

sults for the locus of roots of the own in Fig. 6. In comparison with that the degree of elastic coupling nt in determining whether the ef- or destabilizing. For full elastic e effect is generally highly stabiliz- f lead-lag frequencies considered. t the elastic coupling allows the nergy from the weakly damped in- dc to the well damped flapping e inherently low aerodynamic and amping can easily be augmented er of magnitude. This is significant he inplane degree of freedom is not abilities as its low inherent damp-

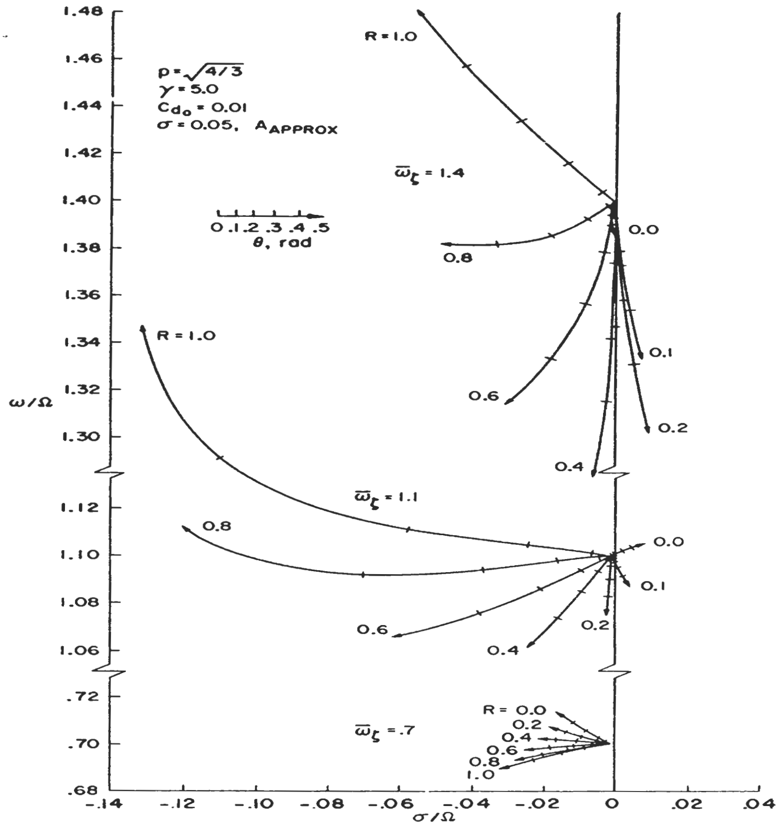


FIGURE 6. Locus of lead-lag mode roots, Case III, rigid blade equations with variable elastic coupling.

($\bar{\omega}_{\zeta} < 1$) rotor blades are only stabilized by elastic coupling. Further evidence is provided by Fig. 7 which presents stability boundaries for variable elastic coupling as a function of inplane frequency with $p = \sqrt{4/3}$. This figure clearly shows that for stiff inplane blades there exists a particular value of $R$ for which instability can occur at moderately low pitch angles but that increased elastic coupling is strongly stabilizing. Furthermore, this minimum pitch angle is equal to $\theta^*$ given by Eq. (13) for the basic flap-lag equations.

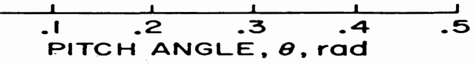


parison of approximations for induced inflow-

$\theta/2$. This approximation eliminates the
amic lead moment in the lead-lag cou-
it $C_{\dot\beta}$.
ful but more accurate approximation for
nflow parameter can be derived as fol-
ıct expression for $A$ is based on non-
ed inflow given by blade-element mo-
y.[6] For $a = 2\pi$

$$\pi\sigma\Omega R/8[\sqrt{1 + 16\theta\xi/\pi\sigma} - 1] \quad (6)$$

mated by the value at $\xi = {}^3/_4$, the follow-
or $A$ results

$$_{\text{ox}} = \pi\sigma/6[\sqrt{1 + 12\theta/\pi\sigma} - 1] \quad (7)$$

of these two approximate expressions is
the exact value in Fig. 1. The effect of
to be important and therefore limits the
$= \theta/2$ for quantitative results. $A_{\text{approx}}$,
ite accurate and will be used for the re-
low
xaı. .ation of flap-lag stability and dy-
v be carried out for several specific cases.
ximate rigid blade equations these in-
flap-lag coupling, 2) the effects of pre-
ble elastic coupling, and 4) pitch-lag
, the results using multimode elastic
s are presented and compared with pre-
ıd finally, the effects of elastic coupling
ponse are examined.

RIGID BLADE STABILITY

*-cone or Elastic Coupling*

v of the basic flap-lag stability charac-
rigid hinged blade is afforded by Fig. 2.

Neutral stability occurs when Routh's discriminant vanishes, i.e.,

$$F = D(BC - AD) - B^2E = 0 \quad (9)$$

After some manipulation the following expression for the collective pitch for neutral stability is obtained.

$$(\theta - A)^2 = \frac{P^2}{2(P-1)(2-P)} \times \left\{D + \frac{[D + A\theta][P - W]^2}{\eta^2[W + P(D + A\theta)][1 + D + A\theta]}\right\} \quad (10)$$

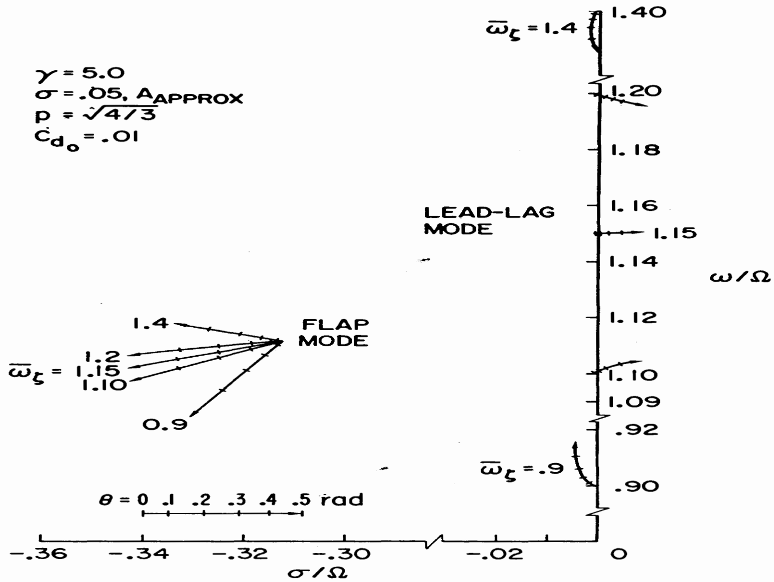


FIGURE 2. Locus of roots for increasing pitch angle, Case I, basic rigid blade equations.

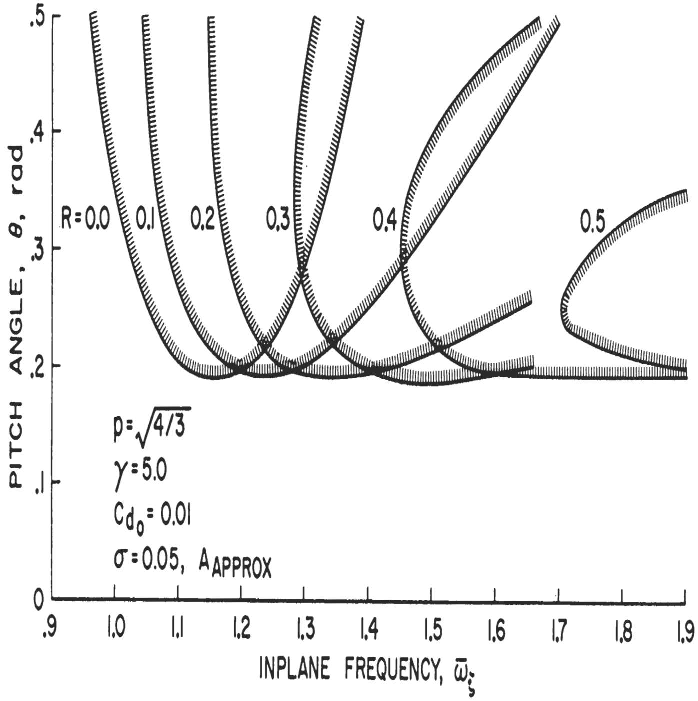


FIGURE 7. Stability boundaries for rigid blade equations with variable elastic coupling.

where

$$P = p^2, W = q^2, Z = z^2 \tag{25}$$

This expression neglects the effect of elastic coupling on $\beta_0$ which is consistent with dropping second order terms in the perturbation analysis. Equation (24) confirms that elastic coupling, $Z$, can be destabilizing; however, it can be shown that $\theta$ cannot be less than $\theta^*$. For small pitch angles ($\theta^2 \ll 1$) Eq. (24) can be greatly simplified yielding

$$(\theta - A)^2 = \frac{P^2}{2(P-1)(2-P)} \times$$

with inplane frequencies differing from $p$ are subject to the same critical stability condition if the elastic coupling is in accord with Eq. (28).

*Case IV, Pitch-lag Coupling*

To provide further information about hingeless rotor blade stability characteristics, a brief examination of the influence of kinematic pitch-lag coupling has been made. Since the important torsional degree of freedom is not included in the present paper, this together with a brief outline of the method of solution. Particular care was required to insure that centrifugal and Coriolis forces which produce the destabilizing flap-lag coupling were retained in the derivation. These forces arise from blade radial displacements and tension variations resulting from perturbation deflections and velocities respectively. These effects are normally not included in elastic rotor blade equations. In addition, they do not have direct counterparts in the approximate rigid blade equations since radial displacements and tension do not appear explicitly in those equations.

Results obtained using the elastic blade modal equations are presented in Fig. 9. The first inplane mode damping is relatively high as a result of the elastic coupling. Because the principle elastic axes of the rotor blade rotate through the pitch angle $\theta$ for the entire length of the blade, the elastic coupling is equivalent to $R = 1.0$ for the rigid blade. The effect of number of the modes retained in the equations is relatively slight as far as the first inplane mode damping is concerned. A single flap and lead-lag mode are denoted by $n = 1$, two of each mode are included for $n = 2$. To illustrate the importance of the proper derivation of the elastic equations, the damping is also shown with the radial displacement and tension perturbations neglected. This gives a very unconservative result since the destabilizing flap-lag terms are not present.

A comparison with the rigid blade damping ($R = 1.0$) shows the approximate equations to be quite ac-

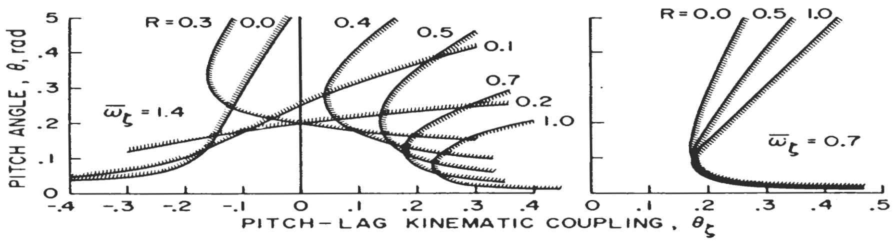


FIGURE 8. Stability boundaries for rigid blade equations, Case IV, kinematic pitch-lag coupling and variable elastic coupling, $p = \sqrt{4/3}$, $\gamma = 5.0$, $c_{d_0} = 0.01$, $\sigma = 0.05$.

Figure 2. Locus of roots for flap-lag equations with stall; $p = \sqrt{4/3}$, $\gamma = 5.0$, $\sigma = 0.05$, $c_{d_p} = 0.01$, $\eta_m = 0.0$.

$$c_l = c_{l_0} + c_{l_\alpha}\Delta\alpha + \ldots + \text{higher order terms}$$
$$c_d = c_{d_0} + c_{d_\alpha}\Delta\alpha + \ldots + \text{higher order terms} \tag{10}$$

If the angle of attack variations associated with flap and lead-lag perturbations are sufficiently small, the higher order terms in the series may be omitted and the aerodynamic coefficients can be specified by four parameters: the equilibrium or steady-state lift and drag coefficients, $c_{l_0}$ and $c_{d_0}$; and the lift and drag curve slopes $c_{l_\alpha}$ and $c_{d_\alpha}$ at the equilibrium angle of attack. These four nonlinear parameters can be incorporated in the linearized equations of motion giving the modified aerodynamic coefficients in Table 1. These coefficients are written in closed form when the angle of attack is constant along the blade radius. Otherwise, the aerodynamic coefficients must be evaluated by numerical spanwise integration for each operating condition. Note that $\phi_l = A_{\text{approx}}$ of Ref. 3 and that the original profile drag coefficient $c_{d_0}$ has been replaced by $c_{d_p}$ to avoid confusion with the present usage where $c_{d_0} = c_{d_0}(\alpha)$. The Coriolis and centrifugal terms in $F_{\dot{\zeta}}$ and $C_{\dot{\beta}}$ appear as $\pm 2\beta_0$ in Table 1 and the percent of critical lead-lag structural damping is denoted by $\eta_m$. All other terms are of aerodynamic origin. The nonlinear coefficients will reduce to their linear counterparts if the appropriate linear aerodynamic values for $c_{l_0}$, $c_{d_0}$, $c_{l_\alpha}$, $c_{d_\alpha}$ are substituted ($c_{l_0} = a\alpha$, $c_{d_0} = c_{d_p}$, $c_{l_\alpha} = a$, $c_{d_\alpha} = 0$, $\alpha = \theta - \phi_l$) and $1 + c_{d_p}/a$ is approximated by 1. Changes in the aerodynamic coefficients due to stall effects are evident from a comparison of the two sets of coefficients in Table 1. The most important effect is the reduction in the flap damping moment, $F_{\dot{\beta}}$, due to the reduction of the local lift curve slope $c_{l_\alpha}$ in the stall regime. In effect, the Lock number varies with angle of attack.

### *Effect of Stall on Stability*

The nonlinear analysis shows that the effect of stall on flap-lag stability is sensitive to the specific rotor blade configuration and operating condition. Typical locus of root plots in Fig. 2 illustrate these results. Simple analytical expressions for the lift and drag curves, typical of the NACA 0012 airfoil section at the low test Reynolds numbers ($Re \simeq 1.5 \times 10^5$) have been used.

$$c_l = 6\alpha - 10\alpha^2,\ c_d = 0.01 + 11.1\alpha^3$$
$$c_{l_\alpha} = 6 - 20\alpha,\ c_{d_\alpha} = 33.3\alpha^2 \tag{11}$$

Three basic configurations are presented in Fig. 2. Linear stability characteristics for these configurations are given in Ref. 3. The soft inplane $\bar{\omega}_\zeta = 0.7$ case generally exhibits a large increase in lead-lag damping and a large decrease in flap damping from stall. Although the flap-mode root is shown

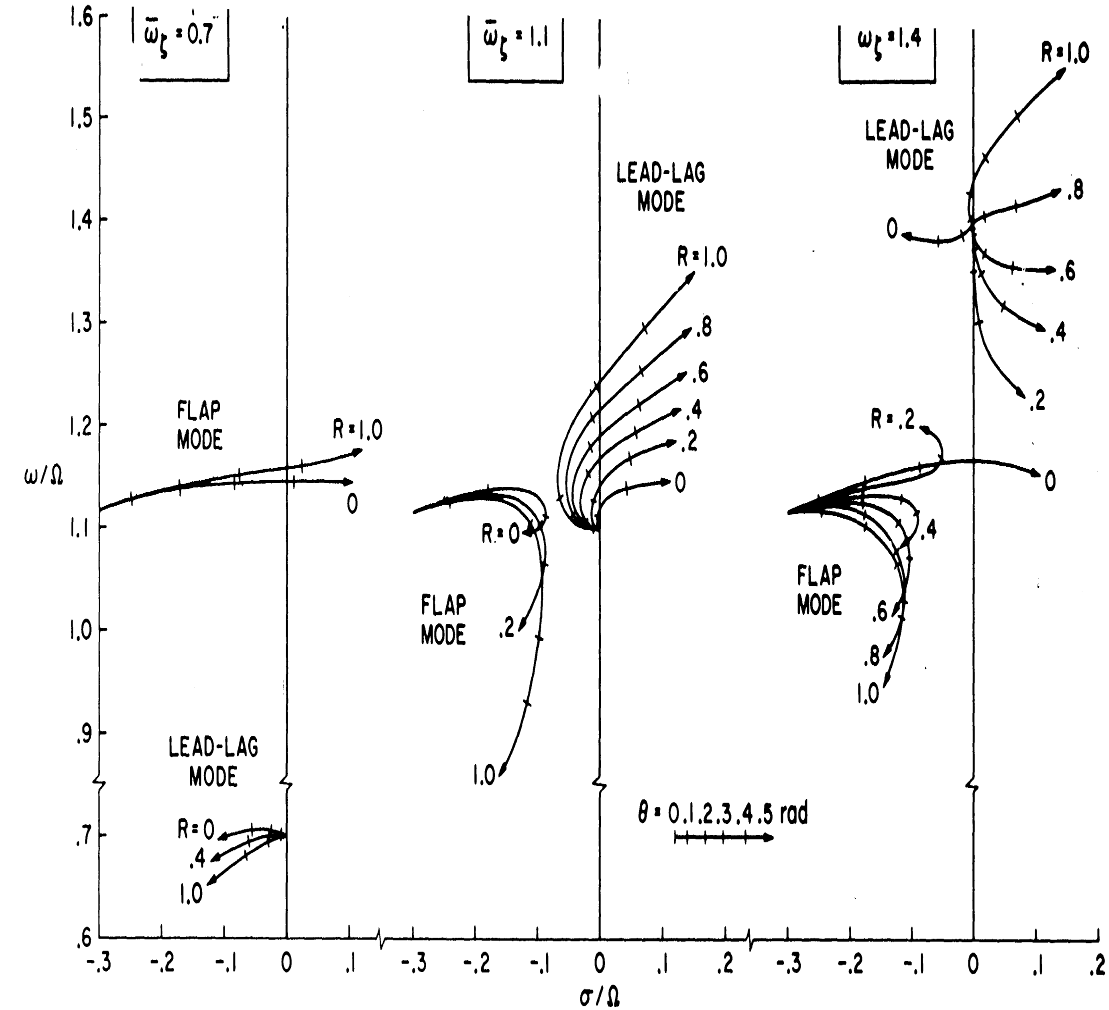


Figure 2. Locus of roots for flap-lag equations with stall; $p = \sqrt{4/3}$, $\gamma = 5.0$, $\sigma = 0.05$, $c_{d_p} = 0.01$, $\eta_m = 0.0$.

$$c_l = c_{l_0} + c_{l_\alpha}\Delta\alpha + \ldots + \text{higher order terms}$$

$$c_d = c_{d_0} + c_{d_\alpha}\Delta\alpha + \ldots + \text{higher order terms} \tag{10}$$

If the angle of attack variations associated with flap and lead-lag perturbations are sufficiently small, the higher order terms in the series may be omitted and the aerodynamic coefficients can be specified by four parameters: the equilibrium or steady-state lift and drag coefficients, $c_{l_0}$, $c_{d_0}$, $c_{l_\alpha}$, $c_{d_\alpha}$ are substituted ($c_{l_0} = a\alpha$, $c_{d_0} = c_{d_p}$, $c_{l_\alpha} = a$, $c_{d_\alpha} = 0$, $\alpha = \theta - \phi_l$) and $1 + c_{d_p}/a$ is approximated by 1. Changes in the aerodynamic coefficients due to stall effects are evident from a comparison of the two sets of coefficients in Table 1. The most important effect is the reduction in the flap damping moment, $F_{\dot\beta}$, due to the reduction of the local lift curve slope $c_{l_\alpha}$ in the stall regime. In effect, the Lock number varies with angle of attack.

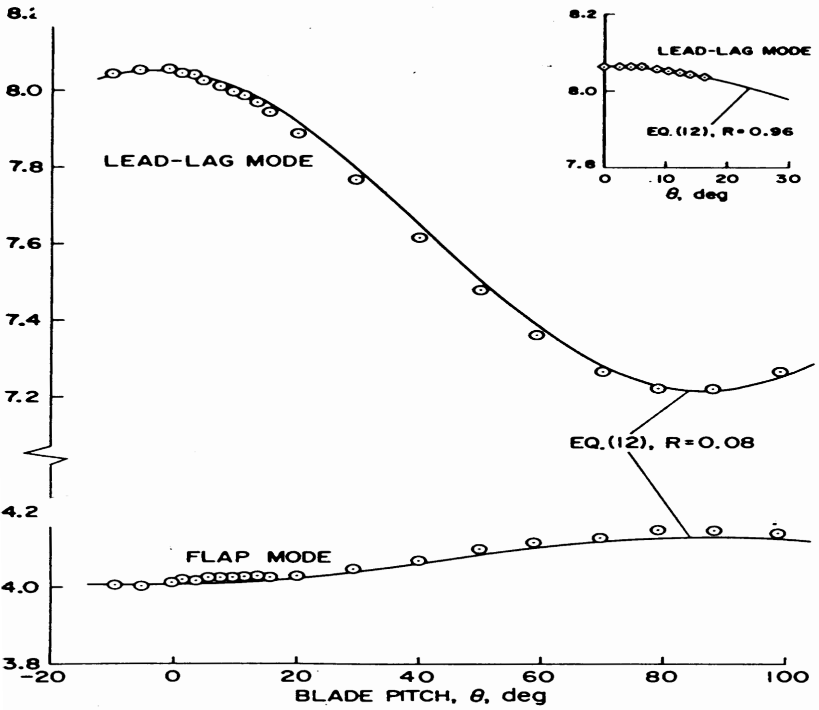


ure 6. Nonrotating flap and lead-lag natural fre-
ncies for weak ($R = 0.08$) and strong ($R = 0.96$,
et) elastically coupled configurations.

given in Fig. 6. The uncoupled frequencies
and $\omega_\beta$ are determined by the maximum and
iimum measured values, respectively, which
ɔ define the zero reference for the effective
ıctural pitch angle $\theta_s$. This angle differs from
ae. ɔdynamic pitch angle measured at the ¾
ius by −3.2° for the weak elastically coupled
figuration because of blade spar twist. For
strong elastically coupled configuration the
odynamic and structural pitch angles are co-

The coupled rotating natural freque
Eq. 1 for the values of $R$ found above
for reference purposes in Fig. 7. At
angle, the flap and lead-lag modes ar
The degree of coupling for nonzero p
depends on $R$. These results show th
resonance with 1/rev excitation occu
speeds near 475 rpm and that couplin
flap and lead-lag modes is strongest
425 rpm. Determination of lead-lag c
difficult at these speeds because of r
and beating effects.

*Steady-State Measurements*

The equilibrium deflections of the b
were measured to determine the stea
stall characteristics of the rotor. Th
ments were used to calculate effectiv
values of the blade lift and drag coeff
$c_d$ vs. angle of attack by assuming a
constant downwash angle $\phi_i$, neglectir
and using a tip loss factor $B = 0.97$.
efficients from the measured data exh
gradual stall, with a low value of max
coefficient, high profile drag, and a ra
rise with angle of attack, all characte
havior for low Reynolds numbers. Vi
servations of stroboscopically illumir
indicated that stall progressed radiall
as pitch angle increased, and the enti
stalled at $\theta = 17°$.

*Lead-Lag Mode Transient Responses*

Examples of the response of the lea

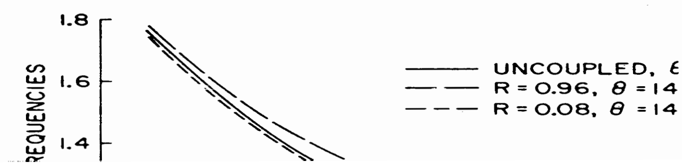

Figure 10. Dimensionless lead-lag damping; $\theta = 10.4°$, $R = 0.96$.

rations. Flagged symbols denote data reduced by the Peak Plot method. The remaining data were manually reduced. Three different analytical results are also included; the uncoupled single degree of freedom lead-lag mode damping, linear flap-lag theory, and flap-lag theory with stall. Figure 9 clearly confirms the destabilizing effect of aerodynamic and inertial flap-lag coupling for the weak elastically coupled configuration. This is shown by the pronounced reduction in damping near 400 rpm compared with the un-

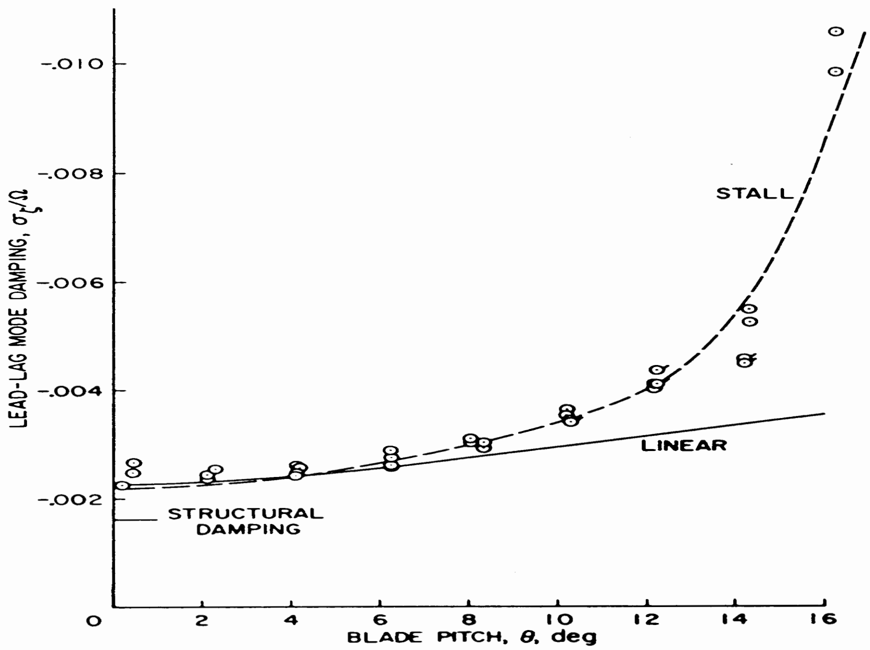


Figure 11. Dimensionless lead-lag damping at 300 rpm; $R = 0.08$, $\bar{\omega}_\zeta = 1.62$, $p = 1.28$.

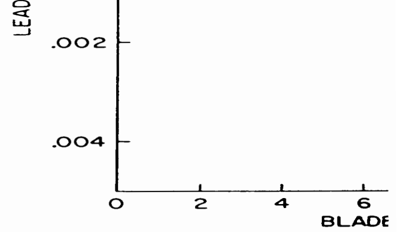


Figure 12. Dimensionless l
$R = 0.08$, $\bar{\omega}_\zeta = 1.21$, $p = 1.$

coupled damping. The ef
evident in Fig. 9. At low
the measured damping is
the stall theory which pr
ing compared to linear t
in damping was measure
inplane case) and althoug
an increased effect of st
not as good. Measureme
unreliable because of $\bar{\omega}_\zeta$
cussed earlier. The disc
rpm is not considered to
it was also present at lo
addition, this discrepanc
accounted for by errors
although the method tend
ing under high noise con
The measured data for
coupled configuration in
the highly stabilizing inf
predicted by theory. The
can be appreciated by co
(note the scale reduction
damping is the same in b
stabilizing at low rpm (s
has little effect at high r
The measured data agre
except in the region whe
is near the flap frequenc
sured results are unrelia

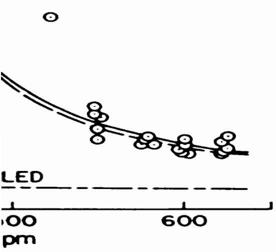


damping; $\theta$ = 10.4°,

te ta reduced
emaining data
different analytical
ncoupled single
le damping, linear
eory with stall.
estabilizing effect
-lag coupling
configuration.
d reduction in
d with the un-

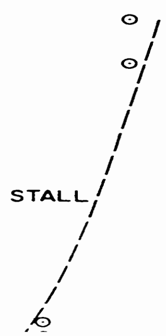


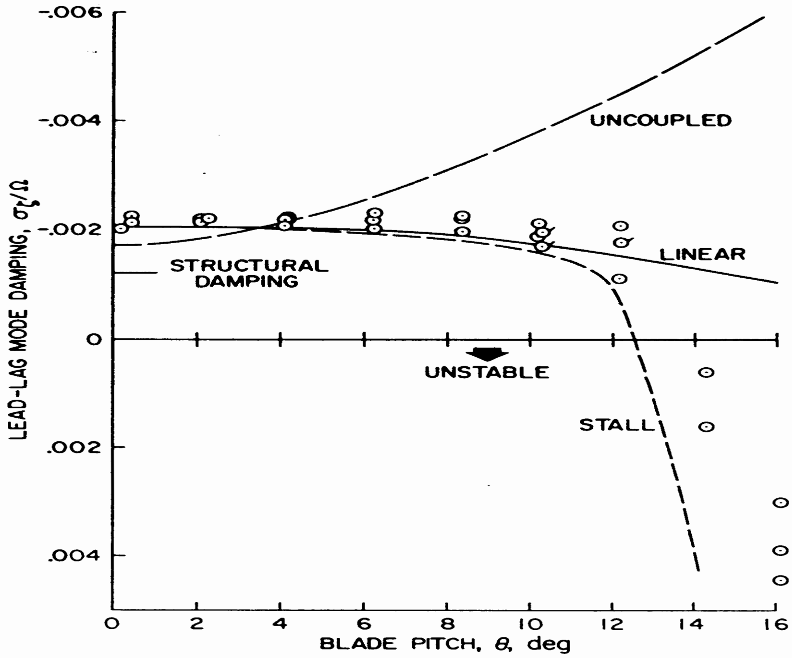


Figure 12. Dimensionless lead-lag damping at 400 rpm; $R = 0.08$, $\bar{\omega}_\zeta = 1.21$, $p = 1.17$.

coupled damping. The effects of stall are also evident in Fig. 9. At low rpm (stiff inplane case) the measured damping is in good agreement with the stall theory which predicted increased damping compared to linear theory. A larger increase in damping was measured for high rpm (soft inplane case) and although stall theory also shows an increased effect of stall, the correlation is not as good. Measurements near 475 rpm are unreliable because of $\bar{\omega}_\zeta$, 1/rev resonance discussed earlier. The discrepancy at the highest rpm is not considered to be due to stall since it was also present at lower pitch angles. In addition, this discrepancy probably cannot be accounted for by errors in the data reduction

ioı clearly evident
pitch angle at various
e weak elastically
tiff inplane, $\bar{\omega}_\zeta = 1.62$),
essive increase in
ood agreement with

coupled case at 400
Fig. 12, stall-induced
pitch angle. At this
ic and inertial flap-lag
inant and their de-
ow stall, is evident
oupled single degree
ng (where the large
to induced drag). A
ement at this test
s stabilizing may have
ec. y the original

upled configuration
nown in Fig. 13. This
ced instability for a
h the elastic coupling
near region below
is completely reversed

REMARKS

l findings have revealed
motion instability
d hingeless rotor con-
er in the stall regime.
instability is unlike
er (dependent on un-
nlinear stall flutter
ping from hysteresis
moment), both of
sional blade deflec-
may be of practical
ential problem areas
e emphasized that the

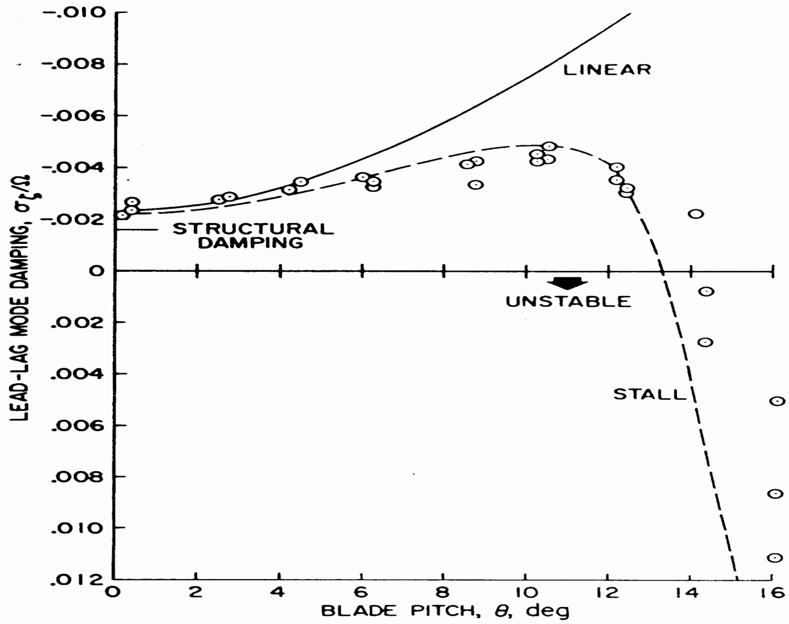


Figure 13. Dimensionless lead-lag damping at 300 rpm; $R = 0.96$, $\bar{\omega}_\zeta = 1.62$, $p = 1.28$.

experimental measurements below stall.

3. The aerodynamic and inertial flap-lag coupling terms of the linear theory were confirmed insofar as the model configuration with small elastic coupling exhibited the predicted reduction in lead-lag mode damping at rotor speeds where lead-lag and flap mode frequencies were nearly equal.

4. Each of the four nonlinear airfoil aerodynamic parameters $c_{l_0}$, $c_{d_0}$, $c_{l_\alpha}$, and $c_{d_\alpha}$ used in linear flap-lag theory were found to contribute significantly to the total effect of stall. The drag curve slope $c_{d_\alpha}$ is usually destabilizing, the drag rise $c_{d_0}$ is stabilizing, and the lift curve slope $c_{l_\alpha}$ may be either stabilizing or destabilizing

paper will be devoted to this problem. Because any increase in lead-lag damping must arise from coupling between flap and lead-lag degrees of freedom, clues to possible approaches may be gained by examining the coupling terms in the equations of motion. At zero pitch angle, the product of the coupling terms in the Laplace transformed flap-lag equations can be written simply, for R = 1, as[7]

$$K = \frac{\omega_\Delta^2}{2} \sin 2\theta_{s_0} \left( \frac{\omega_\Delta^2}{2} \sin 2\theta_{s_0} - \frac{\gamma}{8} \theta_\zeta \right) \qquad (1)$$

Flap-lag structural coupling is characterized mainly by the parameter $\theta_{s_0}$, the inclination of the principal flexural axes of the blade when the blade aerodynamic pitch angle $\theta$ is zero. The parameter $\omega_\Delta^2 = \omega_\zeta^2 - \omega_\beta^2$ is defined by the difference between the nonrotating blade frequencies (or equivalently, the difference between the flap and lead-lag bending stiffnesses) and is also an essential part of flap-lag structural coupling. It may be seen that for $\omega_\Delta^2 \neq 0$, if $\theta_{s_0}$ is nonzero, or $\theta_{s_0}$ and $\theta_\zeta$ are both nonzero, the flap and lead-lag degrees of freedom will be coupled at zero pitch angle. Depending on the sign of K,[7] this coupling will increase (K > 0) or decrease (K < 0) the blade lead-lag damping. If $\theta_{s_0}$ is zero, K will be zero, independent of pitch-lag coupling; therefore pitch-lag coupling alone cannot increase lead-lag damping. If $\theta_\zeta$ is zero, K varies with $\theta_{s_0}^2$ for small $\theta_{s_0}$, and thus flap-lag structural coupling alone will provide only small increases in lead-lag damping. For the couplings to be effective at zero pitch angle, the relation for K indicates that both $\theta_{s_0}$ and $\theta_\zeta$ should be provided, and that $\theta_\zeta$ should be less than zero.

... the variation of lead-lag damping as a function of lead-lag frequency at zero blade pitch angle. It is clear from these results that if the lead-lag frequency is too close to the matched-stiffness value, no significant increase in damping will result. Since the matched-stiffness condition also depends on the blade flap frequency, increasing the flap frequency for a given lead-lag frequency will also reduce the flap-lag structural coupling.

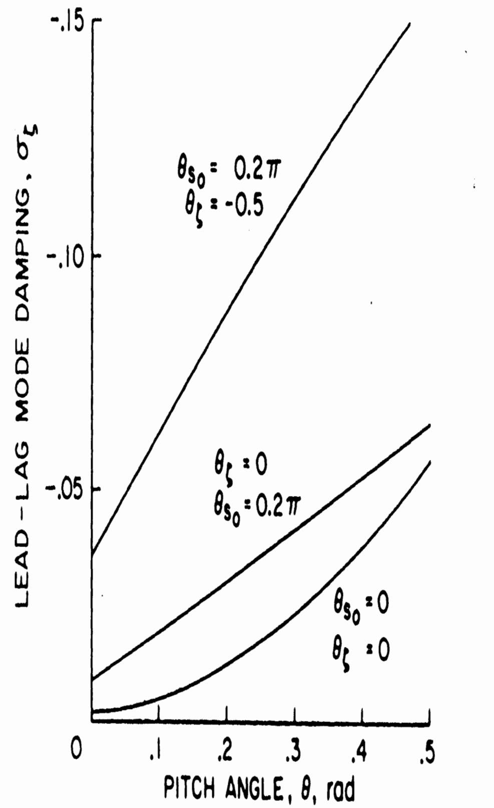


Figure 2. The effect of flap-lag structural coupling and pitch-lag coupling on isolated rigid blade lead-lag mode damping, p = 1.1, $\omega_\zeta = 0.7$, $\gamma = 8$, $\sigma = 0.05$, $c_d = 0.01$.

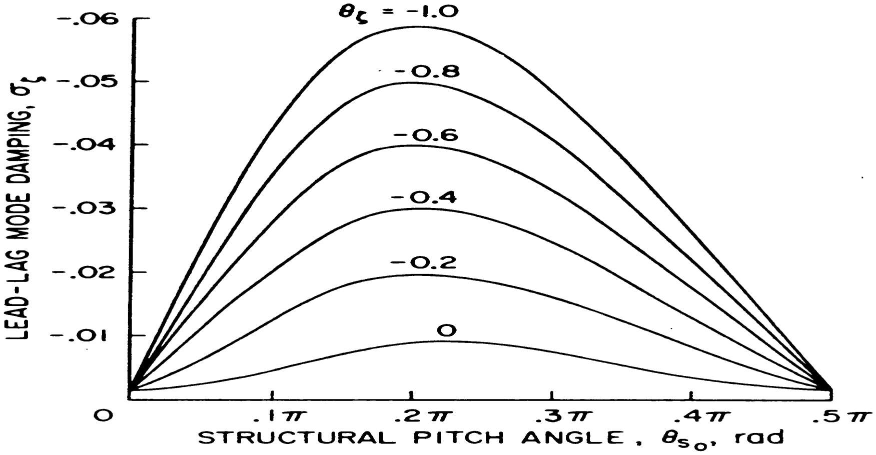


Figure 3. The effect of flap-lag structural coupling and pitch-lag coupling on isolated rigid blade lead-lag mode damping at zero blade pitch angle, $\theta = 0$, $p = 1.1$, $\omega_\zeta = 0.7$, $\gamma = 8$, $\sigma = 0.05$, $c_d = 0.01$.

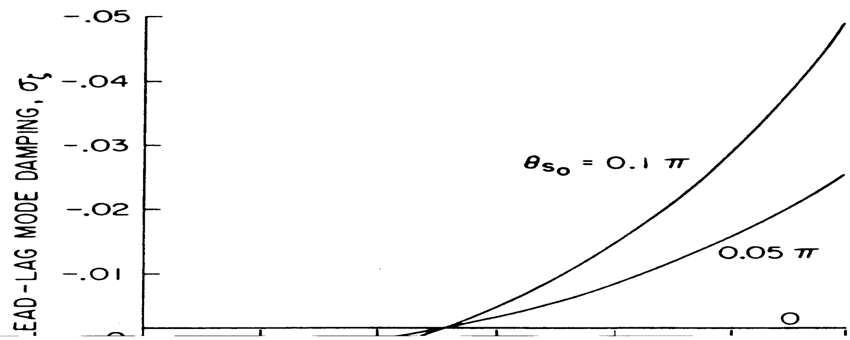


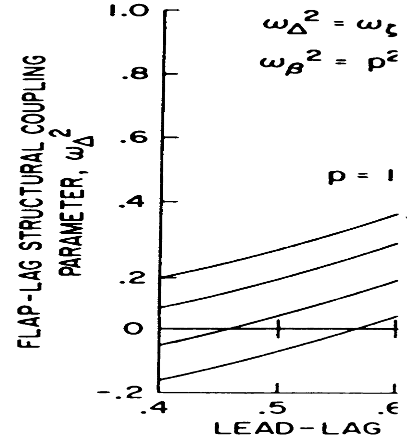


Figure 5. The effect
frequencies on th
tural coupling pa

One consequence o
tural coupling at zero
the coupled natural fr
blade will be modified
an adverse effect on o
of the rotor or rotor-
tions where the uncoup
greater than the match
tion of the principal
the coupled flap frequ
lead-lag frequency, as
coupled natural freque
and they are not great
forces unless pitch-la
introduced. When nega
added to increase the
lag frequency is furth

A final parameter
Lock number. For the

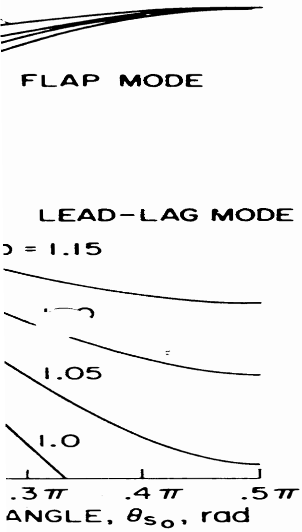


tructural pitch angle
d flap and lead-lag
zeuc) $\omega_\zeta$ = 0.7.

coupling. The struc-
inclining the flex-
ct to the rotor plane
oling was provided by
from axes that would
ne blade radius.

nta[illegible]esults is shown
nd [illegible]edicted lead-lag
ree basic configura-
flap-lag structural
; structural coupling
;perimental results
previous discussion.
discrepancies for

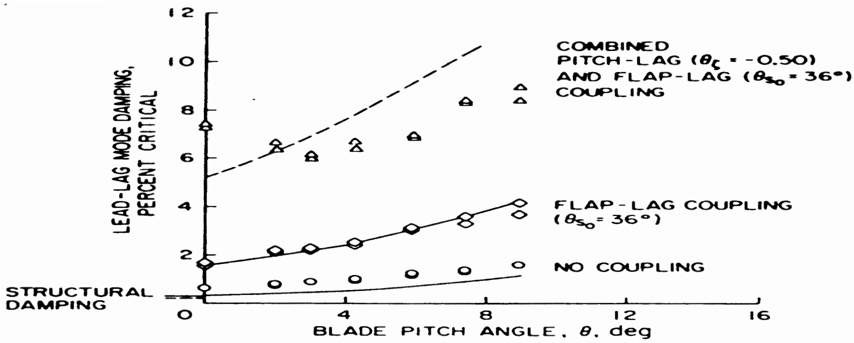


Figure 7. Comparison of experimentally measured lead-lag mode damping with isolated rigid blade theory for a coupled lead-lag mode frequency of 0.7, from Reference 8.

sophisticated analysis becomes necessary. A first step in this direction is to consider an elastic rotor blade with a pitch bearing attached to a rigid hub. Such a configuration may include blade torsional flexibility, pitch-link flexibility, precone, droop, sweep, torque offset, hub offset, twist, and chordwise offsets of the blade mass center, tension axis, elastic axis, and aerodynamic center. In this section we will consider the effects of some — but not all — of these parameters on the stability and lead-lag damping of an isolated rotor blade. It should be noted that even this configuration is not the most general one that may be conceived. One may also consider a somewhat more complex configuration having bending flexibility inboard of the pitch bearing, or a completely bearingless configuration without a pitch bearing at all. In the latter case, the mechanical and structural details of the pitch-changing mechanism play a significant role in determining the aeroelastic properties of the system.

For the purposes of this paper, only the simple hingeless rotor blade configuration with a pitch bearing rigidly attached to the hub will be considered. The development of the mathematical model of this system is described in detail in references 9 and 10. Briefly, the general partial